CHEMISTRY

Evolution of anatase surface active sites probed by in situ sum-frequency phonon spectroscopy

Yue Cao,[1,2] Shiyou Chen,[3,4] Yadong Li,[5] Yi Gao,[5] Deheng Yang,[1,2] Yuen Ron Shen,[1,6]* Wei-Tao Liu[1,2]*

Surface active sites of crystals often govern their relevant surface chemistry, yet to monitor them in situ in real atmosphere remains a challenge. Using surface-specific sum-frequency spectroscopy, we identified the surface phonon mode associated with the active sites of undercoordinated titanium ions and conjoint oxygen vacancies, and used it to monitor them on anatase (TiO$_2$) (101) under ambient conditions. In conjunction with theory, we determined related surface structure around the active sites and tracked the evolution of oxygen vacancies under ultraviolet irradiation. We further found that unlike in vacuum, the surface oxygen vacancies, which dominate the surface reactivity, are strongly regulated by ambient gas molecules, including methanol and water, as well as weakly associated species, such as nitrogen and hydrogen. The result revealed a rich interplay between prevailing ambient species and surface reactivity, which can be omnipresent in environmental and catalytic applications of titanium dioxides.

INTRODUCTION

The reactivity of catalyst surfaces originates from surface active sites (1). For example, titanium dioxide (TiO$_2$) is an inert insulator in its stoichiometric form but becomes a highly active photocatalyst with surface defects (2). A thorough characterization of such active sites, in particular under reaction conditions (3), is indispensable for understanding the reaction mechanisms (1). Vibrational spectroscopy is arguably the most powerful in situ technique for surface analyses and has made substantial contributions to the field of heterogeneous catalysis (4–6). It has been predominantly applied to studies of adsorbates yet provides little information on surface lattice structure (1). The latter can be gleaned from surface vibrational modes or surface phonons, but it is often challenging to detect them because of the concurrence of very intense bulk phonon modes. Of particular interest to catalysis are those surface phonons directly associated with surface reactions; their identification and in situ characterization can provide real-time direct information about the catalytic processes (7–9).

Sum-frequency generation (SFG) has been developed as a surface-specific version of vibrational spectroscopy (10). It can probe not only adsorbates but also surface lattice modes with the bulk response suppressed (11, 12). Here, we report the application of SFG to identify the surface phonon mode connected to active sites on anatase (TiO$_2$) (101) and use it to probe in situ surface reactions at such sites. Titanium dioxide is a benchmark model system in surface science and is also known as one of the most important photocatalysts (13–17). Among the two industrially used polymorphs, rutile and anatase, the latter is regarded catalytically more active, and its (101) surface often appears as the dominant facet in active nanophase materials (18). Recent studies in ultrahigh vacuum (UHV) have revealed a wealth of information on well-defined anatase surfaces (18–24), yet their structures and properties, such as bonding geometries and response to external stimuli, are still not well characterized, especially under ambient reaction conditions. Using SFG, we have successfully identified a surface phonon mode directly associated with the two major surface active sites on anatase (101): the five-coordinated titanium [Ti(5c)] and the oxygen vacancy (V_O^{surf}) on the two-coordinated oxygen [O(2c)] site (Fig. 1A), both being primary adsorption and/or dissociation sites for key reactants (16). This surface phonon can then serve as a spectroscopic signature for reactions on anatase (101). Through characterizing and monitoring this phonon mode, we were able to determine the surface bonding geometry at the active sites and track the creation and annihilation of V_O^{surf} following ultraviolet (UV) irradiation, and found that V_O^{surf}'s could be efficiently stabilized by prevailing ambient gases. In UHV, V_O^{surf} on anatase (101) has been proven unstable (18, 19, 22), which is apparently discordant with the high reactivity of the surface (16, 25). Our result shows that ambient gas can make a big difference in stabilizing V_O^{surf}, which could be of pivotal importance for practical applications.

RESULTS

The surface phonon mode and related bonding geometry

In our experiment, the anatase (101) sample was cleaned and placed in a chamber purged with various gases and could be irradiated in situ by UV light (see Materials and Methods for details). For SFG, the incident 800-nm near-infrared (NIR) and the broadband IR beams overlap on the sample surface and generate the SF vibrational spectrum in reflection. The basic theory of SFG is sketched in the Supplementary Materials. Briefly, when the IR frequency is near the phonon resonance, the SF signal (S_{SF}) is proportional to $|\overleftrightarrow{\chi}_{NR} + \overleftrightarrow{\chi}_R|^2$, where $\overleftrightarrow{\chi}_{NR}$ is the nonresonant background, and $\overleftrightarrow{\chi}_R = \sum_q \dfrac{\overleftrightarrow{A}_q}{\omega_{IR} - \omega_q + i\Gamma_q}$ is the resonant contribution, with $\overleftrightarrow{A}_q$, ω_q, and Γ_q being the amplitude, frequency, and damping coefficient of the qth resonance mode, respectively (11). Our SF vibrational spectrum on anatase (101) taken with PPP polarization combination in the spectral range of 700 to 1000 cm^{-1} is displayed (red curve) in Fig. 1B, in comparison with the Raman spectrum (blue curve) from the

[1]Physics Department, State Key Laboratory of Surface Physics, Key Laboratory of Micro and Nano Photonic Structures [Ministry of Education (MOE)], Fudan University, Shanghai 200433, China. [2]Collaborative Innovation Center of Advanced Microstructures, Nanjing 210093, China. [3]Key Laboratory of Polar Materials and Devices (MOE), East China Normal University, Shanghai 200241, China. [4]Collaborative Innovation Center of Extreme Optics, Shanxi University, Taiyuan, Shanxi 030006, China. [5]Division of Interfacial Water and Key Laboratory of Interfacial Physics and Technology, Shanghai Institute of Applied Physics, Chinese Academy of Sciences, Shanghai 201800, China. [6]Physics Department, University of California, Berkeley, Berkeley, CA 94720, USA.
*Corresponding author. Email: yrshen@berkeley.edu (Y.R.S.); wtliu@fudan.edu.cn (W.-T.L.)
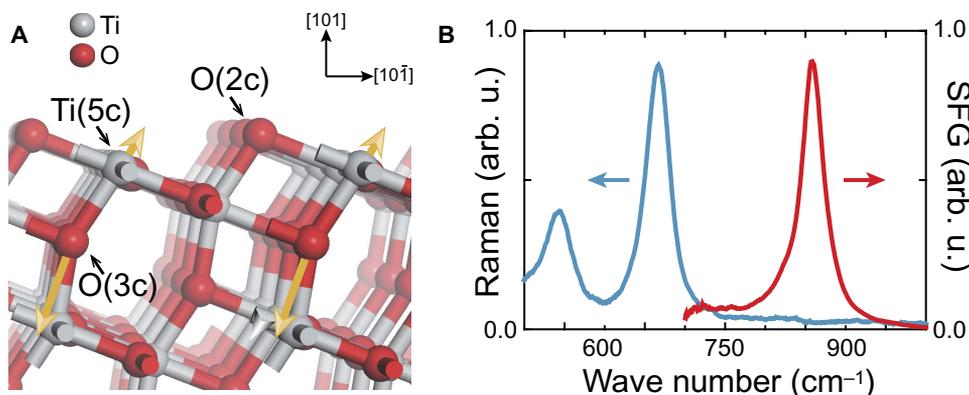
Fig. 1. Structure and phonon spectra of anatase (101). (**A**) Structure of anatase (101). Ti(5c), O(2c), and O(3c) denote five-coordinated titanium and two- and three-coordinated oxygen ions, respectively. Yellow arrows describe the displacements of Ti(5c) and O(3c) associated with the surface phonon mode according to ab initio calculation. (**B**) Raman (blue) and SFG (red) spectra of the anatase (101) sample, with all beams being P-polarized. The two Raman modes are the highest-frequency transverse optical (TO) phonon modes of bulk anatase. The 860-cm^{-1} SFG mode is from the surface. arb. u., arbitrary units.

same sample. The two bands at 543 and 667 cm^{-1} are the two highest-frequency Raman-active TO phonon modes of bulk anatase (*26–28*). In contrast, the SF spectrum exhibits a new resonance at ~860 cm^{-1} from the (101) surface. On the basis of our ab initio calculation that reveals a surface resonance at ~878 cm^{-1} on fully relaxed anatase (101) (see calculation details in the Supplementary Materials), we identify the observed SF mode as mainly due to the stretching vibration of the bond between Ti(5c) and the fully coordinated oxygen ion beneath it [O(3c)] (Fig. 1A and fig. S1). Because Ti(5c) exists predominantly on the surface, this is a highly localized surface phonon mode.

To further confirm the assignment, we checked whether symmetry properties of the 860-cm^{-1} mode agree with that of the assigned surface phonon mode. Anatase (101) belongs to the C_{1v} point group with a mirror plane perpendicular to the [010] axis (Fig. 2A) (*29*). Its phonon modes can be characterized by two irreducible representations, A' and A'', corresponding to transition dipole moments lying parallel and perpendicular to the mirror plane, respectively. The Ti(5c)–O(3c) bonds lie in the mirror plane, and the bond stretching phonon mode transforms according to the A' representation. We measured, for different input/output polarization combinations, the SFG spectra of the 860-cm^{-1} mode versus the azimuthal angle of anatase (101), ϕ, between the incidence plane and the [10$\bar{1}$] axis on the surface [see geometries described in Fig. 2 (A to C)]. At $\phi = 0°$ and 180° (Fig. 2, A and B), the transition dipole moment of an A' mode should be parallel to the incident plane, so it cannot be excited by the S-polarized IR input. On the other hand, it can be excited by the P-polarized IR light, but as the transition dipole moment tilts away from the surface normal (which is essential for the C_{1v} group), the excitation is different for $\phi = 0°$ and 180°, and so is the spectral intensity. As seen in Fig. 2 (D to F), these symmetry features are observed in the SPS, SSP, and PPP spectra of the 860-cm^{-1} mode (see the Supplementary Materials for more details). For $\phi = 90°$ (Fig. 2C) and 270°, the geometries for probing an A' mode are equivalent, and its SF spectra should be the same. This is true within experimental uncertainty for the 860-cm^{-1} mode (SSP spectra are presented in Fig. 2G as an example). Therefore, the result confirms that the 860-cm^{-1} mode is an A' mode expected for the Ti(5c)–O(3c) bond stretching phonon on anatase (101).

The SFG finding allows us to determine related surface structures on anatase (101). The higher surface phonon frequency, compared to

bulk phonons, suggests that the Ti(5c)–O(3c) bond is shorter than bulk counterparts because of surface relaxation. Our calculation finds the former shorter than the latter by ~0.13 Å (*30*). Next, orientation of the Ti(5c)–O(3c) bonds can be deduced from the spectral anisotropy at $\phi = 0°$ and 180° (Fig. 2, E and F). For both SSP and PPP polarization combinations, the intensity ratio of the 860-cm^{-1} mode is given by

$$S_{SF}(\phi = 180°)/S_{SF}(\phi = 0°) \approx |(\mu_{a,\text{eff}} - \mu_{c,\text{eff}})/(\mu_{a,\text{eff}} + \mu_{c,\text{eff}})|^2$$

where $\mu_{a(c),\text{eff}}$ is the effective transition dipole moments along the [10$\bar{1}$] ([101]) axis. We find $|\mu_{a,\text{eff}}/\mu_{c,\text{eff}}| \approx 1.0 \pm 0.2$, from which we deduce the dipole moment to tilt by ~25 ± 5° from the [101] axis, close to the theoretical prediction (see the Supplementary Materials for more details). The agreement further validates our assignment of the 860-cm^{-1} mode and sets the foundation for using it to investigate reactions on anatase (101).

UV-induced surface structural change

Ti(5c) is the major adsorption site on TiO$_2$ for key reactants, such as methanol and water, but how they adsorb is still a subject of debate (*31, 32*). If adsorbed molecules bind strongly to Ti(5c), the corresponding Ti(5c)–O(3c) stretching frequency should exhibit a shift (see the Supplementary Materials). In our experiment, the 860-cm^{-1} mode barely shifted when the clean anatase (101) surface was exposed to saturated methanol vapor. This indicates that methanol was not very tightly bonded to Ti(5c). If adsorbed methanol molecules were dissociated, we would expect that with methoxy as the dissociated fragment bonded to Ti(5c), the corresponding Ti–O stretching mode should have a significant red shift, and the C–H stretching spectrum of methoxy should appear. Neither was observed in our SFG measurement (fig. S2). So, at least at room temperature and high coverage, methanol must have adsorbed on anatase (101) in the molecular form [similar to the case of methanol adsorption on rutile (110) (*31, 32*)]. Methanol dissociation is either not favored, or dissociated fragments would recombine rapidly (*33*). For water, its dissociation upon adsorption is predicted to be even less favorable (*31, 34*).

Upon UV irradiation, methoxy is still not detectable (fig. S2). However, the 860-cm^{-1} phonon intensity dropped sharply (Fig. 3A)
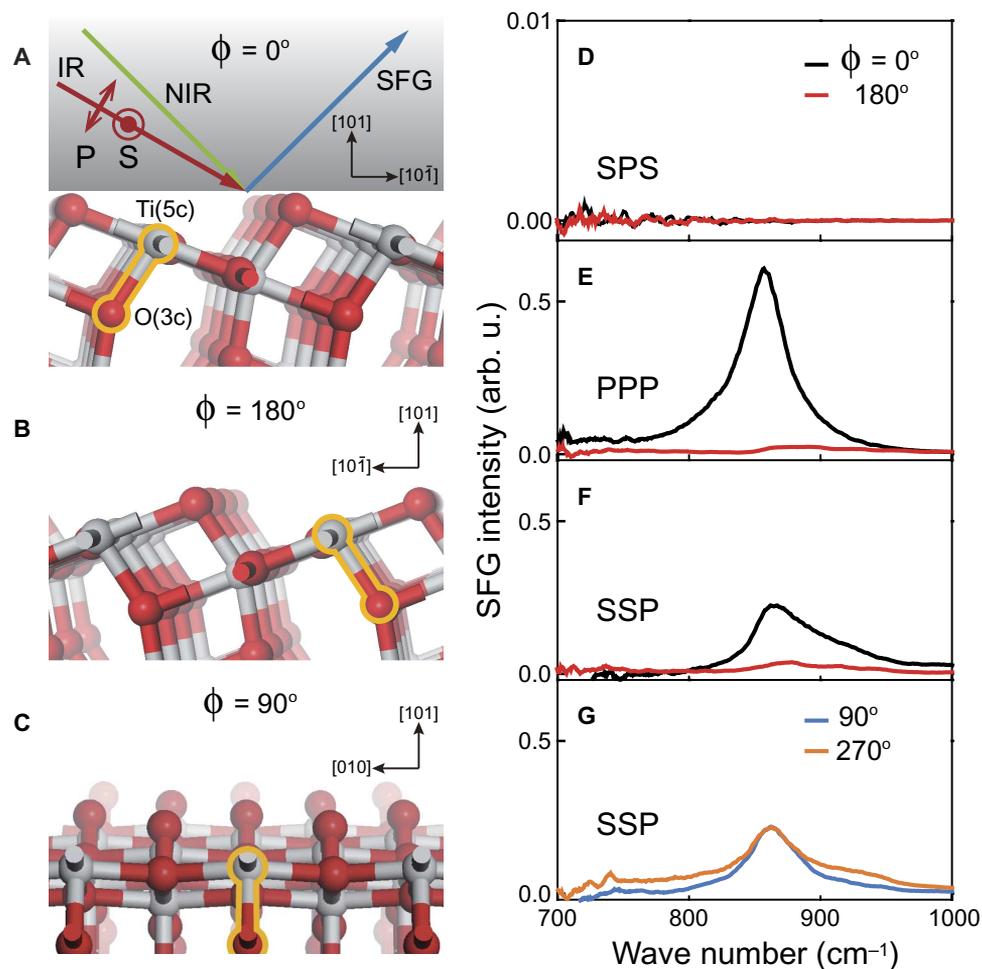
Fig. 2. Symmetry of the surface and phonon spectral anisotropy. (**A** to **C**) Experimental configurations with the sample placed at various azimuthal angle ϕ. The beam incident geometry is as described in (A), with green, red, and blue arrows denoting NIR, IR, and SFG beams, respectively, which are either P- or S-polarized. A Ti(5c)–O(3c) bond is highlighted in yellow at each ϕ. (**D** to **G**) SFG spectra at various ϕ with different beam polarization combinations (labeled in capital letters, referring to the polarization of SFG, NIR, and IR beams from left to right). Black (red) curves in (D) to (F) are spectra taken at $\phi = 0°$ (180°), and the blue (orange) curve in (G) is taken at $\phi = 90°$ (270°).

not only in methanol and water vapors but also in other ambient gases, such as nitrogen and hydrogen. It is known that UV can generate oxygen vacancies on TiO_2 (*14*). For anatase (101), the surface oxygen vacancy, V_O^{surf}, is preferentially formed at the O(2c) site (Fig. 3B), lowering the coordination of the conjoint Ti(5c) to Ti(4c) (*19*, *21*). Accordingly, the number density of Ti(5c) decreases, and so does the intensity of the 860-cm^{-1} mode. To establish that the intensity drop is due to creation of V_O^{surf}, we compared the UV-induced spectral change of anatase (101) in pure oxygen with that in other gases. As shown in Fig. 3C, the UV-induced intensity change of the 860-cm^{-1} mode in oxygen differs markedly from the others: When UV is on, it drops to below 25% in pure nitrogen and methanol vapor but remains as high as 60% in oxygen; when UV is off, the signal recovers to less than 50% in nitrogen and methanol but almost fully in oxygen. In other gases, the spectral changes are similar to those in nitrogen and methanol, but in clear contrast to that in oxygen. Obviously, oxygen is unique because it can directly replenish surface oxygen vacancies. Hence, we conclude that the UV-induced intensity drop of the 860-cm^{-1} mode is predominantly due to the increment of V_O^{surf}'s.

Stabilization of surface oxygen vacancies by ambient gases

We can thus use the 860-cm^{-1} mode to monitor the amount of V_O^{surf} directly under ambient conditions. In UHV, V_O^{surf} is unstable and tends to migrate down to form subsurface vacancies (V_O^{sub}) (Fig. 3B) (*18*, *19*, *22*). Such migration is also evident under ambient conditions. Under UV irradiation, the mode intensity drops upon generation of V_O^{surf} but levels off at a nonzero value (Fig. 3C). This suggests that while V_O^{surf} is being created, it also tends to disappear from the surface by forming V_O^{sub}. The two processes balance each other at a finite number of V_O^{surf} in dynamic equilibrium. When UV is off, creation of V_O^{surf} stops, but the conversion to V_O^{sub} does not, so that the number of V_O^{surf} decays until a new equilibrium is reached between V_O^{surf} and V_O^{sub} (Fig. 3C), depending on their free energy difference. We found this balance differs for different ambient gases. Recently, the enhanced stability of V_O^{surf} on anatase (101) by ambient water vapor was proposed by Li and Gao (*25*). Here, we extend the calculation to cases of methanol, nitrogen, and hydrogen with results shown in Fig. 3D (circles) (see also table S1). The calculated energy difference (ΔE) between V_O^{surf} and V_O^{sub} is found to be as high as +0.46 eV in vacuum, but becomes
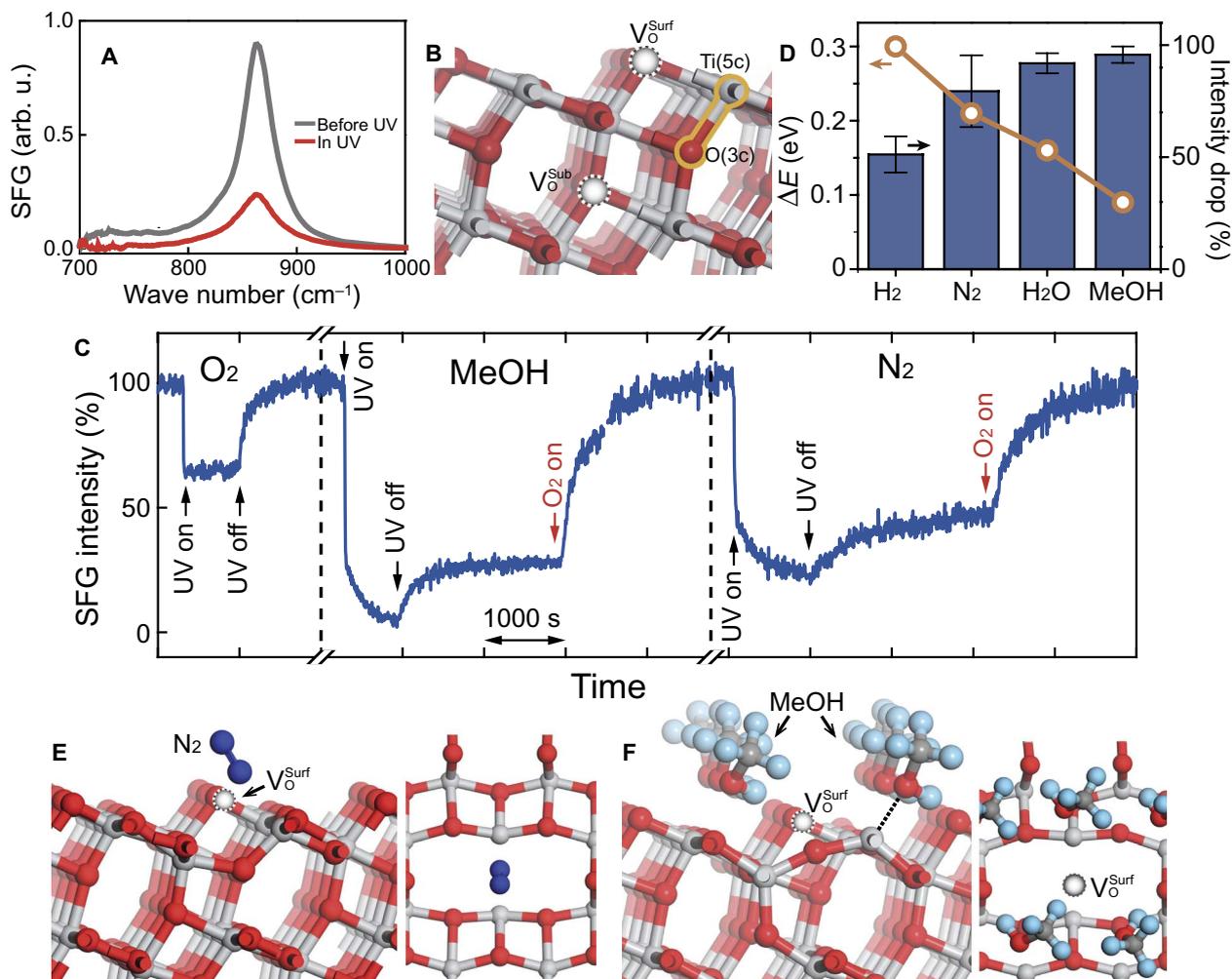
Fig. 3. Evolution of the surface structure in UV and different ambient gases. (**A**) Surface phonon spectra of anatase (101) in pure nitrogen before (blue) and after (green) UV irradiation. (**B**) Preferential locations of surface (V_O^{surf}) and subsurface (V_O^{sub}) oxygen vacancies on anatase (101), marked by dashed circles. (**C**) Evolution of the mode intensity in pure oxygen, saturated methanol vapor, and pure nitrogen in response to switching on and off of UV irradiation as well as oxygen purge. (**D**) Circles indicate energy difference between surface and subsurface oxygen vacancies [$\Delta E = E(V_O^{surf}) - E(V_O^{sub})$] in various ambient gases obtained from ab initio calculation. Vertical columns represent percentage drop of the 860-cm^{-1} mode after a constant UV irradiance in various ambient gases: Pure hydrogen and nitrogen were at ~1 atm; water and methanol were at saturated vapor pressure mixed with dry nitrogen. (**E** and **F**) Stable configurations of methanol and nitrogen molecules adsorbed near a surface oxygen vacancy by ab initio calculation.

+0.30 eV in hydrogen, and is only +0.09 eV in methanol. If we assume that the entropy difference between V_O^{surf} and V_O^{sub} does not depend on the ambient gases, the ranking order of the free energy difference will be the same as that of ΔE. Then, for smaller ΔE, the stability of V_O^{surf} is higher, or the final density of V_O^{surf} is larger. Experimentally, the density of V_O^{surf} can be monitored by the 860-cm^{-1} mode intensity. We plot in Fig. 3D the final percentage drop of the 860-cm^{-1} mode because of persistent V_O^{surf} on anatase (101) in the four ambient gases after the same UV irradiance. It shows that the persistent V_O^{surf} follows the ranking order of methanol→water→nitrogen→hydrogen, correlating nicely with the opposite ranking order of the calculated ΔE.

To understand the underlying physics, we resort to adsorption configurations of gas molecules on anatase (101) (see details in fig. S3). Nitrogen and hydrogen only interact weakly through van der Waals interaction with the anatase surface, but they can still adsorb to V_O^{surf}'s

(Fig. 3E) with a low surface coverage. Methanol and water bind more strongly to anatase (101); they can yield a high surface coverage (Fig. 3F) (31, 34) and slightly dope the surface conduction band with their oxygen lone pair electrons. As discussed by Li and Gao (25), the surface with V_O^{surf} has more electronic density of states near the bottom of the conduction band so that the stability of V_O^{surf} can be enhanced by electron doping. Methanol, in particular, is most efficient in stabilizing V_O^{surf}'s. Because V_O^{surf}'s are regarded as reaction centers on titanium dioxides (25, 35), enhancing the stability of V_O^{surf} may be the reason why methanol appears as a promotional agent in some reactions on anatase (23, 36). As all molecules we have studied are widely present in applications of TiO$_2$ as catalysts, one could anticipate the reactivity in ambient conditions to be very different from that in vacuum. The same is likely to be true on other reactive surfaces of oxides (25).

DISCUSSION

In summary, we have identified a highly localized surface phonon mode of anatase (101), a benchmark photocatalyst surface. This mode is associated with the low-coordinated titanium ions and conjoint oxygen vacancies at the surface. It serves as a spectroscopic signature for direct, in situ monitoring of the active surface sites under reaction conditions. In sharp contrast to the case in vacuum, we found that the stability of surface active sites was strongly regulated by ubiquitous environmental molecules, such as methanol and water; even weakly associated molecules, such as hydrogen and nitrogen, showed an appreciable effect. Our finding not only signifies the urgency of in situ surface characterization but also calls for a more comprehensive view on heterogeneous catalysis: Instead of considering only a surface with reactants on it, the active role played by ambient gases must be seriously taken into account.

MATERIALS AND METHODS

Sample preparation

Anatase (101) samples of 2 mm thick were purchased from SurfaceNet and MaTecK. The MaTecK sample was repolished (by Hefei Kejing Materials Technology Co. Ltd.) to an epi roughness of ~0.4 nm. Both were Fe-doped mineral crystals and yielded consistent experimental results. Before the measurement, samples were ultrasonicated in acetone, ethanol, and deionized water (18.2 megohm·cm) consecutively, followed by UV-ozone treatment for 5 min, which effectively removed organic contaminations as indicated by the SFG spectra from the samples (fig. S4). During the measurement, samples were mounted in a chamber with a base pressure of <10 Pa. Pure nitrogen, oxygen, or hydrogen gas filled the chamber to about 1 atm. Methanol (Sigma-Aldrich, 99%) and water filled the chamber to their saturated vapor pressure.

SFG measurements

For our experiment, the broadband multiplex SF spectroscopy scheme was adopted. A regenerative Ti:Sapphire amplifier (Spitfire, Spectra-Physics) produced ~4 W of 800-nm, 35-fs pulses at 1-kHz repetition rate. About 2.6 W of the beam was used to generate narrowband pulses of ~0.5-nm bandwidth by passing the 35-fs pulses through a Bragg filter (N013-14-A2, OptiGrate). The rest of the amplifier output was used to generate broadband IR pulses (~500 cm^{-1}) centered at about 800 cm^{-1} from an optical parametric amplifier/difference frequency generation system (TOPAS-C, Spectra-Physics). The narrowband 800-nm (pulse energy of ~15 μJ) and broadband IR (0.8 μJ) pulses overlapped at the sample surface with incident angles of 45° and 57°, respectively. The generated SF signal was collected by a spectrograph (Acton SP2300) and recorded on a charge-coupled device camera (Princeton Instrument PyLoN 1340 × 100). Spectra were normalized to that from a silver mirror. All experiments were conducted at room temperature.

UV irradiation

The UV light used in our experiment was generated by a UV light-emitting diode (Shenzhen Height-LED Opto-Electronic Tech Co. Ltd.) with a central wavelength at 368 nm. Its power density was about 20 mW/cm^2.

Ab initio calculations

The calculation of the phonon mode on the anatase (101) surface was performed using the Vienna Ab-Initio Simulation Package code based on the density functional theory formalism with the projector-augmented wave pseudopotentials and an energy cutoff of 400 eV for the plane-wave basis functions. The generalized gradient approximation to the exchange-correlation functional was used with the Perdew-Burke-Ernzerhof parameterization. The (101) surface was simulated using a slab model with 15 Å vacuum layers, and 4 × 12 × 1 Monkhorst-Pack k-point meshes for the Brillouin zone integration of the 1 × 1 surface cell. For calculation on the stability of oxygen vacancies, a (4 × 1) supercell with six O–Ti–O layers was used for molecule adsorption. The lowest bottom layer was fixed to mimic the bulk, and the atoms of other layers were fully relaxed. A vacuum layer of 20 Å was used to exclude the influence of vertical periodic images. Because of the large supercell, k-point sampling was restricted to the Γ point.

SUPPLEMENTARY MATERIALS

Supplementary material for this article is available at http://advances.sciencemag.org/cgi/content/full/2/9/e1601162/DC1

S1. Basic theory of the sum-frequency generation
S2. Calculation of the surface phonon mode of anatase (101)
S3. Symmetry properties and spectral anistropy of the surface phonon mode on anatase (101)
S4. Adsorbed methanol on anatase (101)
S5. Calculation on the stability of oxygen vacancies on anatase (101) exposed to ambient gases
S6. The removal of hydrocarbon contaminants by UV-ozone treatments
fig. S1. The calculated in-phase and out-of-phase surface phonon modes near 880 cm^{-1}.
fig. S2. SFG spectra in the C–H stretching vibration range for adsorbed methanol on anatase (101).
fig. S3. Optimized surface structures of anatase (101) with various ambient molecules.
fig. S4. SFG spectra of anatase (101) in the C–H stretching vibration range for hydrocarbon contaminants before and after UV-ozone treatment.
table S1. Energy difference between V_O^{surf} and V_O^{sub} of anatase (101) in different ambient environment.
References (37, 38)

REFERENCES AND NOTES

1. A. Vimont, F. Thibault-Starzyk, M. Daturi, Analysing and understanding the active site by IR spectroscopy. *Chem. Soc. Rev.* **39**, 4928–4950 (2010).
2. S. Wendt, P. T. Sprunger, E. Lira, G. K. H. Madsen, Z. Li, J. Ø. Hansen, J. Matthiesen, A. Blekinge-Rasmussen, E. Lægsgaard, B. Hammer, F. Besenbacher, The role of interstitial sites in the Ti3d defect state in the band gap of titania. *Science* **320**, 1755–1759 (2008).
3. B. M. Weckhuysen, Preface: Recent advances in the in-situ characterization of heterogeneous catalysts. *Chem. Soc. Rev.* **39**, 4557–4559 (2010).
4. A. Politano, G. Chiarello, G. Benedek, E. V. Chulkov, P. M. Echenique, Vibrational spectroscopy and theory of alkali metal adsorption and co-adsorption on single-crystal surfaces. *Surf. Sci. Rep.* **68**, 305–389 (2013).
5. A. Savara, E. Weitz, Elucidation of intermediates and mechanisms in heterogeneous catalysis using infrared spectroscopy. *Annu. Rev. Phys. Chem.* **65**, 249–273 (2014).
6. F. Zaera, New advances in the use of infrared absorption spectroscopy for the characterization of heterogeneous catalytic reactions. *Chem. Soc. Rev.* **43**, 7624–7663 (2014).
7. V. E. Henrich, P. A. Cox, *The Surface Science of Metal Oxides* (Cambridge Univ. Press, 1994), 478 pp.
8. D. M. Herlihy, M. M. Waegele, X. Chen, C. D. Pemmaraju, D. Prendergast, T. Cuk, Detecting the oxyl radical of photocatalytic water oxidation at an n-SrTiO₃/aqueous interface through its subsurface vibration. *Nat. Chem.* **8**, 549–555 (2016).
9. T. Nomoto, A. Sasahara, H. Onishi, Optically excited near-surface phonons of TiO₂ (110) observed by fourth-order coherent Raman spectroscopy. *J. Chem. Phys.* **131**, 084703 (2009).
10. Y. R. Shen, Surface nonlinear optics [Invited]. *J. Opt. Soc. Am. B* **28**, A56–A66 (2011).
11. W.-T. Liu, Y. R. Shen, Surface vibrational modes of α-quartz(0001) probed by sum-frequency spectroscopy. *Phys. Rev. Lett.* **101**, 016101 (2008).
12. W.-T. Liu, Y. R. Shen, Sum-frequency spectroscopy on bulk and surface phonons of noncentrosymmetric crystals. *Ann. Phys.* **523**, 101–106 (2011).
13. B. O'Regan, M. Grätzel, A low-cost, high-efficiency solar cell based on dye-sensitized colloidal TiO₂ films. *Nature* **353**, 737–740 (1991).
14. A. Fujishima, X. Zhang, D. A. Tryk, TiO₂ photocatalysis and related surface phenomena. *Surf. Sci. Rep.* **63**, 515–582 (2008).

15. M. A. Henderson, A surface science perspective on TiO₂ photocatalysis. *Surf. Sci. Rep.* **66**, 185–297 (2011).

16. U. Diebold, The surface science of titanium dioxide. *Surf. Sci. Rep.* **48**, 53–229 (2003).

17. W. A. Tisdale, K. J. Williams, B. A. Timp, D. J. Norris, E. S. Aydil, X.-Y. Zhu, Hot-electron transfer from semiconductor nanocrystals. *Science* **328**, 1543–1547 (2010).

18. M. Setvin, U. Aschauer, P. Scheiber, Y.-F. Li, W. Hou, M. Schmid, A. Selloni, U. Diebold, Reaction of O₂ with subsurface oxygen vacancies on TiO₂ anatase (101). *Science* **341**, 988–991 (2013).

19. P. Scheiber, M. Fidler, O. Dulub, M. Schmid, U. Diebold, W. Hou, U. Aschauer, A. Selloni, (Sub)surface mobility of oxygen vacancies at the TiO₂ anatase (101) surface. *Phys. Rev. Lett.* **109**, 136103 (2012).

20. Z. Wang, X. Hao, S. Gerhold, Z. Novotny, C. Franchini, E. McDermott, K. Schulte, M. Schmid, U. Diebold, Water adsorption at the tetrahedral titania surface layer of SrTiO₃(110)-(4 x 1). *J. Phys. Chem. C* **117**, 26060–26069 (2013).

21. M. Setvin, C. Franchini, X. Hao, M. Schmid, A. Janotti, M. Kaltak, C. G. Van de Walle, G. Kresse, U. Diebold, Direct view at excess electrons in TiO₂ rutile and anatase. *Phys. Rev. Lett.* **113**, 086402 (2014).

22. Y. He, O. Dulub, H. Cheng, A. Selloni, U. Diebold, Evidence for the predominance of subsurface defects on reduced anatase TiO₂(101). *Phys. Rev. Lett.* **102**, 106105 (2009).

23. C. Xu, W. Yang, Q. Guo, D. Dai, M. Chen, X. Yang, Molecular hydrogen formation from photocatalysis of methanol on anatase-TiO₂(101). *J. Am. Chem. Soc.* **136**, 602–605 (2014).

24. Y. Wang, H. Sun, S. Tan, H. Feng, Z. Cheng, J. Zhao, A. Zhao, B. Wang, Y. Luo, J. Yang, J. G. Hou, Role of point defects on the reactivity of reconstructed anatase titanium dioxide (001) surface. *Nat. Commun.* **4**, 2214 (2013).

25. Y. Li, Y. Gao, Interplay between water and TiO₂ anatase (101) surface with subsurface oxygen vacancy. *Phys. Rev. Lett.* **112**, 206101 (2014).

26. T. Ohsaka, F. Izumi, Y. Fujiki, Raman spectrum of anatase, TiO₂. *J. Raman Spectrosc.* **7**, 321–324 (1978).

27. R. J. Gonzalez, R. Zallen, H. Berger, Infrared reflectivity and lattice fundamentals in anatase TiO₂s. *Phys. Rev. B* **55**, 7014–7017 (1997).

28. K. Ishioka, H. Petek, Raman generation of coherent phonons of anatase and rutile TiO₂ photoexcited at fundamental absorption edges. *Phys. Rev. B* **86**, 205201 (2012).

29. S. Nakamura, K. Matsuda, T. Wakasugi, E. Kobayashi, G. Mizutani, S. Ushioda, T. Sekiya, S. Kurita, Optical second-harmonic generation from the anatase TiO₂ (101) face. *J. Lumin.* **87–89**, 862–864 (2000).

30. A. Vittadini, A. Selloni, F. P. Rotzinger, M. Grätzel, Structure and energetics of water adsorbed at TiO₂ anatase 101 and 001 surfaces. *Phys. Rev. Lett.* **81**, 2954–2957 (1998).

31. A. Tilocca, A. Selloni, Methanol adsorption and reactivity on clean and hydroxylated anatase(101) surfaces. *J. Phys. Chem. B* **108**, 19314–19319 (2004).

32. S. Liu, A.-a. Liu, B. Wen, R. Zhang, C. Zhou, L.-M. Liu, Z. Ren, Coverage dependence of methanol dissociation on TiO₂(110). *J. Phys. Chem. Lett.* **6**, 3327–3334 (2015).

33. Q. Guo, C. Xu, Z. Ren, W. Yang, Z. Ma, D. Dai, H. Fan, T. K. Minton, X. Yang, Stepwise photocatalytic dissociation of methanol and water on TiO₂(110). *J. Am. Chem. Soc.* **134**, 13366–13373 (2012).

34. A. Tilocca, A. Selloni, Structure and reactivity of water layers on defect-free and defective anatase TiO₂(101) surfaces. *J. Phys. Chem. B* **108**, 4743–4751 (2004).

35. S. Wendt, J. Matthiesen, R. Schaub, E. K. Vestergaard, E. Lægsgaard, F. Besenbacher, B. Hammer, Formation and splitting of paired hydroxyl groups on reduced TiO₂(110). *Phys. Rev. Lett.* **96**, 066107 (2006).

36. T. Kawai, T. Sakata, Photocatalytic hydrogen production from liquid methanol and water. *J. Chem. Soc. Chem. Commun.* 694–695 (1980).

37. Y. R. Shen, *The Principles of Nonlinear Optics* (Wiley-Interscience, 2003), 563 pp.

38. N. Asong, F. Dukes, C.-y. Wang, M. J. Shultz, The effect of iron doping on the adsorption of methanol on TiO₂ probed by sum frequency generation. *Chem. Phys.* **339**, 86–93 (2007).

Science Advances

Evolution of anatase surface active sites probed by in situ sum-frequency phonon spectroscopy

Yue Cao, Shiyou Chen, Yadong Li, Yi Gao, Deheng Yang, Yuen Ron Shen and Wei-Tao Liu

ARTICLE TOOLS	http://advances.sciencemag.org/content/2/9/e1601162
SUPPLEMENTARY MATERIALS	http://advances.sciencemag.org/content/suppl/2016/09/26/2.9.e1601162.DC1
REFERENCES	This article cites 35 articles, 3 of which you can access for free http://advances.sciencemag.org/content/2/9/e1601162#BIBL
PERMISSIONS	http://www.sciencemag.org/help/reprints-and-permissions

Use of this article is subject to the Terms of Service